


Article

On Efficiency of Two-Degree-of-Freedom Galloping Energy Harvesters with Two Transducers

Filip Sarbinowski * and Roman Starosta 

Institute of Applied Mechanics, Faculty of Mechanical Engineering, Poznan University of Technology,
60-965 Poznań, Poland; roman.starosta@put.poznan.pl

* Correspondence: filip.sarbinowski@put.poznan.pl

Abstract: This paper examines the energy efficiency of three variations of the two-degree-of-freedom transverse galloping energy harvester. These variants differ in the number and placement of electromechanical transducers. By utilizing the harmonic balance method, the limit cycles of mathematical models of the devices were determined. Analytical expressions derived from the models were then used to formulate the efficiency of the systems. It was demonstrated that efficiency depends on flow speed and can be comprehensively characterized by the following criteria parameters: peak efficiency, denoting the maximum efficiency of the system, and high-efficiency bandwidth, which describes the range of flow speeds within which the efficiency remains at no less than 90% of peak efficiency. The values of these parameters are heavily reliant on two other parameters: the speed at which the system achieves peak efficiency, referred to as the nominal speed, and also the flow speed at which the system undergoes Hopf bifurcation, namely the critical speed. Comparative analysis revealed that only the device equipped with two electromechanical transducers can potentially outperform a simple one-degree-of-freedom system. For selected parameters, this gain reached nearly 10%.

Keywords: energy harvesting; transverse galloping; harmonic balance method; nonlinear dynamics; flow-induced vibration



Citation: Sarbinowski, F.; Starosta, R. On Efficiency of Two-Degree-of-Freedom Galloping Energy Harvesters with Two Transducers. *Appl. Sci.* **2024**, *14*, 5427. <https://doi.org/10.3390/app14135427>

Academic Editors: Ahmed Elkafas, Gabriele Maria Lozito and Bogdan-Gabriel Burduhos

Received: 9 May 2024
Revised: 17 June 2024
Accepted: 18 June 2024
Published: 22 June 2024



Copyright: © 2024 by the authors. Licensee MDPI, Basel, Switzerland. This article is an open access article distributed under the terms and conditions of the Creative Commons Attribution (CC BY) license (<https://creativecommons.org/licenses/by/4.0/>).

1. Introduction

The ongoing energy crisis and burgeoning concept of the Internet of Things (IoT) [1] are continually motivating factors for researchers from various scientific fields to develop newer technologies that enable cheaper and more efficient generation of usable energy. Among the most innovative of these technologies are those that allow energy recovery from vibrations induced by flow. A commercial example of this is the Vortex Bladeless power plants [2], whose vibrations are excited by von Karman vortices. According to the manufacturer, the cost of energy production using these turbines is only 70% of the cost associated with traditional wind turbines of comparable size [2]. Moreover, their sleek, bladeless design allows for closer placement than standard turbines, facilitating more efficient use of wind farm space.

The discussed advantages of vortex-induced vibration energy harvesters may be partially overshadowed by a significant limitation. Due to their reliance on resonance with the vortex frequency, these devices can generate energy only within a narrow flow speed range. An alternative type of power plant without this limitation is the galloping energy harvester (GEH). Transverse galloping [3] is a phenomenon where vibrations are induced due to the flow separation from a bluff body with an appropriate shape, leading to negative, speed-dependent aerodynamic (hydrodynamic) damping. When the flow speed exceeds a critical value, the negative aerodynamic (hydrodynamic) damping surpasses structural damping, resulting in the overall damping in the system becoming negative. In this situation, the damping will supply energy to the system rather than dissipate it, causing the system to become unstable.

The key advantage of using transverse galloping as an excitation mechanism for energy harvesters is that, beyond the critical speed, the amplitude of oscillation increases indefinitely with the flow speed and remains independent of the frequency or the presence of von Karman vortices.

Early studies [4] explore its potential for energy harvesting, emphasizing the crucial role of aerodynamic coefficients in its efficiency. Subsequent research [5] delves into analytical, numerical, and experimental analyses of GEHs, indicating the detrimental impact of structural damping on the performance of the device.

Due to the critical importance of the aerodynamics of the flowing body, many subsequent works have been devoted to examining the efficiency provided by GEHs of various shapes. Building on this trend, it has been demonstrated, for instance in [6], that rhomboidal shapes exhibit a significant propensity for galloping. The article [7] is dedicated to the study of the properties of a device equipped with a bluff body in the shape of various variants of an isosceles triangle. Furthermore, research [8,9] shows that adding a stream splitter favors power generation. The studies [10–12] have also demonstrated the benefits of employing non-typical shapes. According to the reports presented in [13–16], the efficiency of a GEH can also be increased by giving its surface an appropriate geometric metastructure.

Another extensively investigated area in the development of GEHs is the examination of the impact of nonlinear elasticity on its performance. Studies [17,18] propose a method for analyzing the effect of the nonlinear elasticity coefficient on the characteristics of Hopf bifurcation. The study [19] focuses on improving the energy harvesting performance of galloping systems through the use of magnetic coupling. Conversely, the work [20] presents modeling and experimental investigations of asymmetric distances using magnetic coupling based on a galloping piezoelectric energy harvester, aiming to enhance the stability of the generated power. In the articles [21,22], it has been demonstrated that incorporating nonlinear stiffness into the system can significantly increase its efficiency. Research [23] demonstrates that a GEH composed of two oscillators coupled by a nonlinear magnetic interaction can exhibit a lower critical speed. Furthermore, an appropriate selection of the distance between the magnetic segments can contribute to an increase in the system's efficiency. A similar coupling, but in reference to a single-degree-of-freedom system, was discussed in [24]. This approach resulted in a tristable system, which exhibited an efficiency over 35% greater than that of a standard GEH.

According to the literature, enhancing the energy extraction efficiency of a GEH can be also achieved by extending its mechanical structure with an additional degree of freedom. In [25], two variants of GEHs with two degrees of freedom (GEH2Ds), differing in the location of the applied aerodynamic force, were compared to a single-degree-of-freedom device. Experimental comparisons of the electric voltage generated by the variants were presented in [26] and extended to numerical studies of systems with up to three additional masses in [27]. Comprehensive analytical studies of the voltage generated by a GEH2D, considering the possibility of two different vibration modes, were presented in [28]. A two-mass system, whose segments are magnetically coupled, was discussed in [29]. It was demonstrated that such a system can exhibit both a reduced critical speed and enhanced efficiency.

The literature review clearly indicates that extending the mechanical structure to include an additional degree of freedom is seen as a potential way to increase the efficiency of a GEH. However, the literature does not discuss the fact that within the family of two-mass systems, three device variants can be distinguished, differing in the placement of the electromechanical transducer: it can be located between the stationary base and the first mass, between the masses, or in both of these places.

The aim of this work is therefore to analytically examine the efficiency of all three GEH2D variants, compare them, and assess whether any of them can exhibit greater efficiency than the device of basic design.

2. Efficiency of Reference Variant

While the primary focus of this study lies in analyzing the efficiency of systems with two degrees of freedom, understanding the characteristics of this class of devices can be facilitated by comparing them with a system possessing well-established properties—a linear device with one degree of freedom, hereafter referred to as the reference device (Figure 1). Therefore, it is justified to conduct an analysis of the efficiency of this system, particularly as we aim to highlight a certain intriguing feature of this variant, which has not been previously addressed in the literature. According to articles [3,4], the mathematical model of a GEH takes the form shown in Equation (1) with parameters detailed in Table 1.

$$\hat{m}\ddot{z} + \hat{c}\dot{z} + \hat{k}z - \theta\dot{\xi} = \hat{F}_L(\hat{u}) = -\frac{1}{2}\hat{\rho}\hat{u}^2\hat{h}\left(a_1\frac{\dot{z}}{\hat{u}} + a_3\left(\frac{\dot{z}}{\hat{u}}\right)^3\right), \tag{1a}$$

$$\hat{C}_p\dot{\xi} + \frac{\xi}{\hat{R}} + \hat{\theta}\dot{x} = 0. \tag{1b}$$

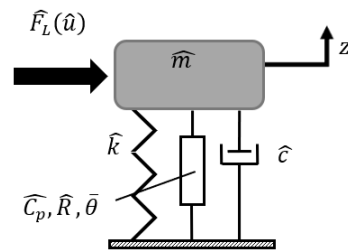


Figure 1. Rodel of reference variant.

Table 1. List of GEH parameters.

Symbol	Parameter	Unit
\hat{m}	Mass	kg
\hat{k}	Stiffness coefficient	N/m
\hat{c}	Damping coefficient	kg/s
\hat{u}	Flow speed	m/s
$\hat{\rho}$	Planar fluid density	kg/m ²
\hat{h}	Characteristic dimension	m
$\hat{\theta}$	Piezoelectric coefficient	N/V
\hat{C}_p	Equivalent capacity	F
\hat{R}	Circuit electrical resistance	Ω
τ	Time	s
$z = z(\tau)$	Vibration vs. time function	m
$\xi = \xi(\tau)$	Voltage vs. time function	V

The efficiency η of such a system is defined as the ratio of the average power generated by the device \hat{P}_g over a time period equal to the period \hat{T} of the voltage function $\xi(\tau)$ to the surface flow power density \hat{P}_f :

$$\eta^L = \frac{\hat{P}_g}{\hat{P}_f} = \frac{\frac{1}{\hat{T}} \int_0^{\hat{T}} \frac{\xi^2(\tau)}{\hat{R}} d\tau}{\frac{1}{2}\hat{\rho}\hat{h}\hat{u}^3}, \tag{2}$$

By introducing the following dimensionless quantities:

$$y = \frac{z}{\hat{h}}, v = \xi \frac{\hat{\theta}}{\hat{m} \hat{h} \hat{\omega}_n^2}, \hat{\omega}_n = \sqrt{\frac{\hat{k}}{\hat{m}}}, c = \frac{\hat{c}}{\hat{m} \hat{\omega}_n}, u = \frac{\hat{u}}{\hat{h} \hat{\omega}_n}, \rho = \hat{\rho} \frac{\hat{h}^2}{2\hat{m}}, r = \hat{C}_p \hat{R} \hat{\omega}_n, \tag{3}$$

$$\kappa = \frac{\hat{\theta}^2}{\hat{C}_p \hat{m} \hat{\omega}_n^2}, t = \tau \hat{\omega}_n,$$

the device dimensionless mathematical model can be written as

$$\ddot{y} + c\dot{y} + y - v = \rho \left(a_1 u \dot{y} + a_3 \frac{\dot{y}^3}{u} \right), \tag{4a}$$

$$\dot{v} + \frac{v}{r} + \kappa \dot{y} = 0. \tag{4b}$$

Assuming that T_c is the period of the function $v(t)$, efficiency in terms of dimensionless parameters can be expressed as

$$\eta^L = \frac{\frac{1}{T_c} \int_0^{T_c} \frac{v^2(t)}{\kappa r} dt}{\rho u^3}. \tag{5}$$

To characterize the efficiency η^L of the system, it is essential to derive the voltage function $v(t)$ generated by it, which can be accomplished using the harmonic balance method. Consequently, it was assumed that the limit cycle of the system would be described by a set of solutions in the following form:

$$y = A_y \cos(\omega t), \tag{6a}$$

$$v = A_v \cos(\omega t + \varphi), \tag{6b}$$

where the four unknown quantities A_y , A_v , $\omega = \frac{\hat{\omega}}{\hat{\omega}_n}$, and φ represent the dimensionless vibration amplitude, dimensionless voltage amplitude, dimensionless vibration frequency, and the phase shift between the oscillator vibrations and voltage oscillations, respectively. The parameter $\hat{\omega}$ denotes the unknown dimensional frequency of the system's vibrations. Substituting solutions of the form Equation (6) into the model Equation (1) leads to the transformation of the system of differential equations into a system of algebraic equations:

$$A_y(1 - \omega^2)\cos(\omega t) + A_y^3 \frac{\rho \omega^3 a_3}{u} \sin^3(\omega t) + A_y \omega (u \rho a_1 - c) \sin(\omega t) - A_v \cos(\omega t + \varphi) = 0, \tag{7a}$$

$$A_v \left(\frac{\cos(\omega t + \varphi)}{r} - \omega \sin(\omega t + \varphi) \right) - A_y \kappa \omega \sin(\omega t) = 0. \tag{7b}$$

This condition will be satisfied for every moment of time t if and only if the sum of the coefficients with corresponding time functions equals zero. From Equation (7b), the following was deduced:

$$\frac{A_v(\cos(\varphi) - r\omega \sin(\varphi))}{r} = 0, \tag{8a}$$

$$\frac{A_v(r\omega \cos(\varphi) + \sin(\varphi)) + A_y \kappa r \omega}{r} = 0. \tag{8b}$$

Equation (8a) shows that

$$\text{tg}(\varphi) = \frac{1}{\omega r}, \quad \sin(\varphi) = \frac{1}{\sqrt{(\omega r)^2 + 1}}, \quad \cos(\varphi) = \frac{\omega r}{\sqrt{(\omega r)^2 + 1}}. \tag{9}$$

Based on Equation (8b) and Equation (9), the expression describing the relationship between the vibration amplitude and the voltage amplitude can be derived:

$$A_v = -A_y \frac{r\kappa\omega}{\sqrt{1 + r^2\omega^2}}. \tag{10}$$

By balancing the harmonics of Equation (7a), the remaining two algebraic equations necessary to determine an approximate solution of the device model are obtained. After

the previously derived relations Equations (9) and (10) are taken into account, they take the form

$$A_y k_e^L \omega - A_y (\omega^2 - 1) = 0, \tag{11a}$$

$$A_y u \rho \omega a_1 + A_y^3 \frac{3\rho \omega^3 a_3}{4u} - A_y c \omega - A_y e^L \omega = 0, \tag{11b}$$

where $k_e^L = \kappa \frac{r^2 \omega^2}{1+r^2 \omega^2}$ and $e^L = \kappa \frac{r}{1+r^2 \omega^2}$ are the piezoelectric stiffness and electrical damping of the linear system. Based on the above system of equations, it can be shown that

$$\omega_1^2 = \frac{r^2(1 + \kappa) - 1 \pm \sqrt{4r^2 + (r^2(1 + \kappa) - 1)^2}}{2r^2} \tag{12a}$$

$$A_y^2 = \frac{4u(c + e^L - u\rho a_1)}{3\rho \omega^2 a_3}. \tag{12b}$$

Equation (12a) shows that $\omega_2^2 < 0$, regardless of the system parameters. Therefore, in the following part of the work, the notation $\omega_1 = \omega$ has been adopted. Returning now to the general definition of efficiency Equation (5) and substituting the expressions Equations (6b), (10), and (12) into it, we obtain

$$\eta^L = \frac{2e^L(c + e^L - u\rho a_1)}{3u^2 \rho^2 a_3}. \tag{13}$$

Figure 2 illustrates the efficiency characteristics of the system. The efficiency is depicted as the ratio η^L / η_p^L , and this representation is maintained throughout the study. The figure also includes the analogous characteristic obtained numerically for initial conditions $y(0) = 0.1, \dot{y}(0) = 0, n(0) = 0$, utilizing the fourth-order Runge–Kutta method.

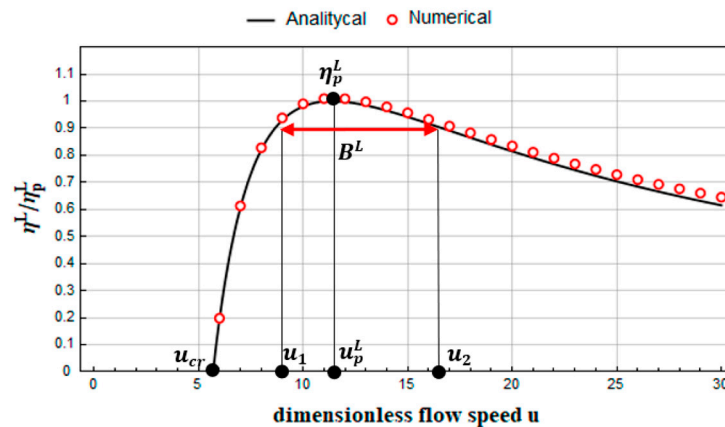


Figure 2. Efficiency characteristics of GEH for $\kappa = 1.3, r = 3, c = 0.1, \rho = 0.02, a_1 = 2.3, a_3 = -18$.

In this figure, it can be observed that the system undergoes Hopf bifurcation at a certain speed, from now on referred to as the critical flow speed u_{cr} . Its value results directly from Equation (13):

$$\eta^L = \frac{2e^L(c + e^L - u\rho a_1)}{3u^2 \rho^2 a_3} = 0 \Rightarrow u = u_{cr} = \frac{c + e^L}{\rho a_1}, \tag{14}$$

Another noteworthy observation from the same set of graphs is that irrespective of the parameter set, there exists a specific nominal flow speed $u = u_p^L$ for which the efficiency η^L

attains a maximum value, denoted as the peak efficiency η_p^L . These quantities are given by the expressions

$$\frac{\delta\eta^L}{\delta u} = 0 \Rightarrow u = u_p^L = 2\frac{c + e^L}{\rho a_1} = 2u_{cr}, \tag{15}$$

$$\eta_p^L = \eta^L(u_p^L) = \frac{-a_1^2 e^L}{6a_3(c + e^L)}. \tag{16}$$

The aforementioned identities were previously derived in [3,4]. However, the remainder of the article discusses entirely original content. An unexplored property of GEHs, which can be inferred from Figure 2 or deduced from the identity $u_p^L = 2u_{cr}$, is noteworthy. A system with a low critical speed u_{cr} will experience a more pronounced decline in efficiency due to the deviation of the flow speed u at which it operates from the nominal speed u_p^L . Let the measure of this phenomenon be the flow speed bandwidth in which the system efficiency η^L does not fall below 90% of the maximum efficiency η_p^L , hereafter referred to as the high-efficiency band B^L . According to the definition, B^L is given as

$$\eta^L = 0.9\eta_p^L \Rightarrow \frac{u_2}{u_1} = \frac{20 \pm 4\sqrt{10}}{9} \frac{(c + e^L)}{\rho a_1}, \tag{17}$$

$$B^L = u_2 - u_1 = \frac{4\sqrt{10}}{9} \frac{(c + e^L)}{\rho a_1} \approx 1.4u_{cr} \approx 0.7u_p^L. \tag{18}$$

The quantities critical speed u_{cr} , nominal speed u_p^L , peak efficiency η_p^L , and high-efficiency bandwidth B^L (Figure 2) will be further referred to as the criterion parameters.

3. Efficiency of Two-Degree-of-Freedom System

According to the information provided in Section 1, the presence of additional mass in systems with two degrees of freedom implies the necessity to consider the placement of the electromechanical transducer. It may be positioned between the main mass and the stationary base (Figure 3a), between the masses (Figure 3b), or in both locations (Figure 3c).

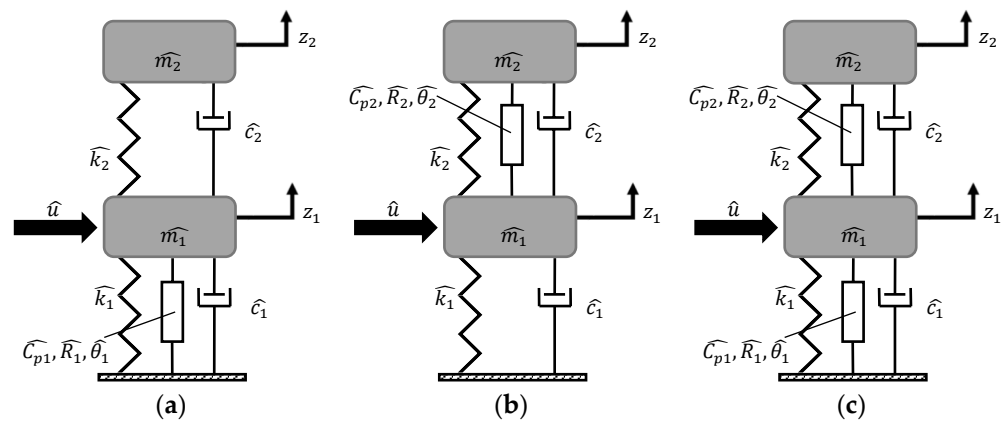


Figure 3. Subvariants of two-degree-of-freedom system: (a) transducer between base and lower mass, (b) transducer between masses, (c) two transducer.

To evaluate the influence of piezoelectric placement on efficiency, the efficiency characteristics of the variant with both transducers will be derived. Subsequently, the consequence of the absence of one of them will be examined.

The dynamics of devices within the discussed category can be described by a general dimensionless mathematical model of the form Equation (20). In addition to the identities in Equation (3), the following also holds:

$$y_i = \frac{z_i}{h}, v_i = \zeta \frac{\hat{\theta}_i}{m_i h \hat{\omega}_n^2}, c_i = \frac{\hat{c}_i}{\hat{m}_1 \hat{\omega}_n}, k_2 = \frac{\hat{k}_2}{\hat{k}_1}, \kappa = \frac{\hat{\theta}_1^2}{C_p i \hat{m}_1 \hat{\omega}_n^2}, \theta = \frac{\hat{\theta}_1}{\hat{\theta}_2}, M = \frac{\hat{m}_2}{\hat{m}_1}, i = 1, 2 \tag{19}$$

$$\ddot{y}_1 + y - k_2(y_2 - y_1) + c_1 \dot{y}_1 - c_2(\dot{y}_2 - \dot{y}_1) - v_1 + v_2 = \rho \left(a_1 u \dot{y}_1 + a_3 \frac{\dot{y}_1^3}{u} \right), \tag{20a}$$

$$\kappa_1 \dot{v}_1 + \frac{v_1}{r_1} + \dot{y}_1, \tag{20b}$$

$$M \ddot{y}_2 + k_2(y_2 - y_1) + c_2(\dot{y}_2 - \dot{y}_1) - v_2 = 0, \tag{20c}$$

$$\kappa_2 \dot{v}_2 + \frac{v_2}{r_2} + \dot{y}_2 - \dot{y}_1 = 0. \tag{20d}$$

To derive the solutions of the GEH2D mathematical model, the procedure outlined in [28] was adapted. It was assumed that the approximate solution of the model Equation (20) will have the following form:

$$y_1 = A_1 \cos(\omega_1 t) + B_1 \sin(\omega_1 t) + G_1 \cos(\omega_2 t) + H_1 \sin(\omega_2 t), \tag{21a}$$

$$v_1 = n_1 \cos(\omega_1 t) + n_2 \sin(\omega_1 t) + n_3 \cos(\omega_2 t) + n_4 \sin(\omega_2 t), \tag{21b}$$

$$y_2 = A_2 \cos(\omega_1 t) + B_2 \sin(\omega_1 t) + G_2 \cos(\omega_2 t) + H_2 \sin(\omega_2 t), \tag{21c}$$

$$v_2 = \vartheta_1 \cos(\omega_1 t) + \vartheta_2 \sin(\omega_1 t) + \vartheta_3 \cos(\omega_2 t) + \vartheta_4 \sin(\omega_2 t), \tag{21d}$$

Substituting the above identities into Equations (20b) and (20d) and then balancing the harmonics $\cos(\omega_1 t)$, $\sin(\omega_1 t)$, $\cos(\omega_2 t)$, $\sin(\omega_2 t)$ allows for the derivation of the relationships between the amplitudes of voltage and the amplitudes of vibration.

$$n_1 = B_1 \omega_1 \varepsilon_{D11} - A_1 \delta_{D11}, \quad n_2 = -A_1 \omega_1 \varepsilon_{D11} - B_1 \delta_{D11}, \tag{22a}$$

$$n_3 = H_1 \omega_2 \varepsilon_{D12} - G_1 \delta_{D12}, \quad n_4 = -G_1 \omega_2 \varepsilon_{D12} - H_1 \delta_{D12},$$

$$\begin{aligned} \vartheta_1 &= \theta(\varepsilon_{D21}(\theta B_2 - B_1)\omega_1 + \delta_{D21}(A_1 - \theta A_2)), \\ \vartheta_2 &= \theta(\varepsilon_{D21}(A_1 - \theta A_2)\omega_1 + \delta_{D21}(B_1 - \theta B_2)), \\ \vartheta_3 &= \theta(\varepsilon_{D22}(\theta H_2 - H_1)\omega_2 + \delta_{D22}(G_1 - \theta G_2)), \\ \vartheta_4 &= \theta(\varepsilon_{D22}(G_1 - \theta G_2)\omega_2 + \delta_{D22}(H_1 - \theta H_2)). \end{aligned} \tag{22b}$$

where $\delta_{Dij} = \kappa_i \frac{r^2 \omega_j^2}{1+r^2 \omega_j^2}$ and $\varepsilon_{Dij} = \kappa_i \frac{r}{1+r^2 \omega_j^2}$ represent the piezoelectric stiffness and electric damping of the i -th piezoelectric for vibration with the j -th frequency.

Harmonic balancing of $\cos(\omega_1 t)$ and $\sin(\omega_1 t)$ of the algebraic equation obtained by substituting the solutions of Equation (21) into Equation (20c) and using the identities Equation (22) leads to the following system of equations:

$$A_2 = B_1 p_1 + A_1 q_1, \tag{23a}$$

$$B_2 = B_1 q_1 - A_1 p_1, \tag{23b}$$

where

$$p_1 = \frac{(k_2 + \theta \delta_{D21})(c_2 + \theta^2 \varepsilon_{D21})\omega_1 - (c_2 + \theta \varepsilon_{D21})(k_2 + \theta^2 \delta_{D21} - M\omega_1^2)\omega_1}{(c_2 + \theta^2 \varepsilon_{D21})^2 \omega_1^2 + (k_2 + \theta^2 \delta_{D21} - M\omega_1^2)^2}, \tag{23c}$$

$$q_1 = \frac{(c_2 + \theta \varepsilon_{D21})(c_2 + \theta^2 \varepsilon_{D21})\omega_1^2 + (k_2 + \theta \delta_{D21})(k_2 + \theta^2 \delta_{D21} - M\omega_1^2)}{(c_2 + \theta^2 \varepsilon_{D21})^2 \omega_1^2 + (k_2 + \theta^2 \delta_{D21} - M\omega_1^2)^2}. \tag{23d}$$

By substituting the above identities into the harmonic balance equations for $\cos(\omega_1 t)$ and $\sin(\omega_1 t)$ of expression (20a), the following identities can be formulated:

$$A_1 \alpha_1 + B_1 \beta_1 - A_1 \frac{3\rho a_3 \omega_1 ((A_2^2 + B_2^2)\omega_1^2 + 2(G_2^2 + H_2^2)\omega_2^2)}{4u} = 0, \tag{24a}$$

$$A_1 \beta_1 - B_1 \alpha_1 + B_1 \frac{3\rho a_3 \omega_1 ((A_2^2 + B_2^2)\omega_1^2 + 2(G_2^2 + H_2^2)\omega_2^2)}{4u} = 0, \tag{24b}$$

where

$$\alpha_1 = \left(p_1 (k_2 + \theta^2 \delta_{D21}) + (c_1 + \varepsilon_{T11} + (c_2 + \varepsilon_{D21})(1 - \theta q_1))\omega_1 - u\rho\omega_1 a_1 \right), \tag{25a}$$

$$\beta_1 = 1 + \delta_{T11} + (\delta_{D21}\theta + k_2)(1 - \theta q_1) - \omega_1 \left(p_1 (c_2 + \theta^2 \varepsilon_{D21}) + \omega_1 \right). \tag{25b}$$

Adapting the above procedure to balance the harmonics $\cos(\omega_2 t)$ and $\sin(\omega_2 t)$ of Equations (20c) and (20a) allows for the derivation of the following identities:

$$G_2 = H_1 p_2 + G_1 q_2, \tag{26a}$$

$$H_2 = H_1 q_2 - G_1 p_2, \tag{26b}$$

$$G_1 \alpha_2 + H_1 \beta_2 - G_1 \frac{3\rho a_3 \omega_2 (2(A_1^2 + B_1^2)\omega_1^2 + (G_1^2 + H_1^2)\omega_2^2)}{4u} = 0 \tag{26c}$$

$$G_1 \beta_2 - H_1 \alpha_2 + H_1 \frac{3\rho a_3 \omega_2 (2(A_1^2 + B_1^2)\omega_1^2 + (G_1^2 + H_1^2)\omega_2^2)}{4u} = 0 \tag{26d}$$

where

$$p_2 = \frac{(k_2 + \theta \delta_{D22})(c_2 + \theta^2 \varepsilon_{D22})\omega_2 - (c_2 + \theta \varepsilon_{D22})(k_2 + \theta^2 \delta_{D22} - M\omega_2^2)\omega_2}{(c_2 + \theta^2 \varepsilon_{D22})^2 \omega_2^2 + (k_2 + \theta^2 \delta_{D22} - M\omega_2^2)^2}, \tag{27a}$$

$$q_2 = \frac{(c_2 + \theta \varepsilon_{T22})(c_2 + \theta^2 \varepsilon_{D22})\omega_2^2 + (k_2 + \theta \delta_{D22})(k_2 + \theta^2 \delta_{D22} - M\omega_2^2)}{(c_2 + \theta^2 \varepsilon_{D22})^2 \omega_2^2 + (k_2 + \theta^2 \delta_{D22} - M\omega_2^2)^2}, \tag{27b}$$

$$\alpha_2 = \left(p_2 (k_2 + \theta^2 \delta_{D22}) + (c_1 + \varepsilon_{T12} + (c_2 + \varepsilon_{T22})(1 - \theta q_2))\omega_2 - u\rho\omega_2 a_1 \right), \tag{27c}$$

$$\beta_2 = 1 + \delta_{D12} + (\delta_{D22}\theta + k_2)(1 - \theta q_2) - \omega_2 \left(p_2 (c_2 + \theta^2 \varepsilon_{D22}) + \omega_2 \right). \tag{27d}$$

By adding Equation (24a) multiplied by B_1 to Equation (24b) multiplied by A_1 , an expression was obtained that allows the frequency ω_1 to be explicitly formulated:

$$1 + k_2 + \delta_{D11} - k_2 q_1 + \delta_{D21}\theta(1 - \theta q_1) - p_1 (c_2 + \theta^2 \varepsilon_{D21})\omega_1 - \omega_1^2 = 0. \tag{28}$$

Similarly, by adding Equation (26c) multiplied by H_1 to Equation (26d) multiplied by G_1 , an equation was obtained from which the frequency ω_2 can be derived:

$$1 + k_2 + \delta_{D12} - k_2 q_2 + \delta_{D22}\theta(1 - \theta q_2) - p_2 (c_2 + \theta^2 \varepsilon_{D22})\omega_2 - \omega_2^2 = 0. \tag{29}$$

Note that in each pair of parameters (p_1, p_2) , (q_1, q_2) , $(\varepsilon_{D21}, \varepsilon_{D22})$, $(\delta_{D11}, \delta_{D12})$, $(\delta_{D21}, \delta_{D22})$, the only difference is the frequency in their definition— ω_1 or ω_2 . Considering the similarity between Equations (28) and (29), one can conclude that the frequencies ω_1 and ω_2 must be equal, thereby excluding the possibility of polymodal vibrations in the system. The expression describing the vibration frequency $\omega_2 = \omega_1$ can therefore be derived by solving only one of the above equations.

The relationship between the vibration amplitude and the system frequency remains unknown. The first of the equations necessary to determine this relationship was obtained by subtracting Equation (24b) multiplied by B_1 from Equation (24a) multiplied by A_1 . The second one is the difference of Equation (26c) multiplied by G_1 and Equation (26d) multiplied by H_1 :

$$p_1(k_2 + \theta^2 \delta_{D21}) + (c_1 + c_2(1 - q_1) + \varepsilon_{D11} + \varepsilon_{D21}\theta(1 - \theta q_1))\omega_1 - u\rho\omega_1 a_1 - \frac{3\rho\omega_1(A_y^2\omega_1^2 + 2G_y^2\omega_2^2)a_3}{4u} = 0, \tag{30a}$$

$$p_2(k_2 + \theta^2 \delta_{D22}) + (c_1 + c_2(1 - q_1) + \varepsilon_{D12} + \varepsilon_{D22}\theta(1 - \theta q_2))\omega_2 - u\rho\omega_2 a_1 - \frac{3\rho\omega_2(2A_y^2\omega_1^2 + G_y^2\omega_2^2)a_3}{4u} = 0, \tag{30b}$$

where $A_y^2 = A_1^2 + B_1^2$ and $G_y^2 = G_1^2 + H_1^2$. The set of Equation (30) has three non-trivial solutions in terms of A_y^2 and G_y^2 , which, after recalling the $\omega_2 = \omega_1$ identity, take the following form:

$$A_y^2 = \frac{4u(p_1(k_2 + \theta^2 \delta_{D21}) + (c_1 + c_2(1 - q_1) + \varepsilon_{D11} + \varepsilon_{D21}\theta(1 - \theta q_1)) - u\rho a_1)}{3\rho\omega_1^3 a_3}, \tag{31a}$$

$$G_y^2 = 0$$

$$A_y^2 = 0, \tag{31b}$$

$$A_y^2 = 0,$$

$$G_y^2 = \frac{4u(p_1(k_2 + \theta^2 \delta_{D21})\omega_1 + (c_1 + c_2(1 - q_1) + \varepsilon_{D11} + \varepsilon_{D21}\theta(1 - \theta q_1)) - u\rho a_1)}{3\rho\omega_1^3 a_3},$$

$$A_y^2 = \frac{4u(3p_1(k_2 + \theta^2 \delta_{D21})\omega_1 + c_1 + c_2(1 - q_1) + \varepsilon_{D11} + \varepsilon_{D21}\theta(1 - \theta q_1)) - u\rho a_1}{9\rho\omega_1^2 a_3}, \tag{31c}$$

$$G_y^2 = \frac{4u(-3p_1(k_2 + \theta^2 \delta_{D21})\omega_1 + c_1 + c_2(1 - q_1) + \varepsilon_{D11} + \varepsilon_{D21}\theta(1 - \theta q_1)) - u\rho a_1}{9\rho\omega_1^2 a_3}.$$

These expressions, along with the previously derived identities, enable the explicit formulation of solutions for the system Equation (20) in the form Equation (21). It should be noted that the identities given by Equations (31a) and (31b) correspond to the same solution in the form of Equation (21); thus, only one of them, namely Equation (31a), will be further analyzed. Moreover, no set of system parameters and initial conditions has been found that would lead to the excitation of vibrations with amplitude Equation (31c). Therefore, this solution was considered unstable, and the efficiency has been derived based only on Equation (31a):

$$\eta_D = \frac{\frac{1}{T_c} \int_0^{T_c} \left(\frac{v_1^2(t)}{r_1 \kappa_1} + \frac{v_2^2(t)}{r_2 \kappa_2} \right) dt}{\rho u^3} = \frac{2\lambda(\mu - u\rho a_1)}{3u^2 \rho^2 a_3}, \tag{32}$$

where

$$\lambda = \left(\varepsilon_{D11} + \varepsilon_{D12}\theta^2 \left(1 - 2\theta q_1 + \theta^2 (p_1^2 + q_1^2) \right) \right), \tag{33a}$$

$$\mu = (c_1 + (c_2 + \theta\varepsilon_{D11})(1 - \theta q_1)) + \frac{p_1(k_2 + \theta^2 \delta_{TD21})}{\omega_1}. \tag{33b}$$

The critical speed u_{cr}^D and nominal speed u_p^D of the GEH2D are given by the following expressions:

$$\eta_D = \gamma_1 \frac{2\lambda(\mu - u\rho a_1)}{3u^2 \rho^2 a_3} = 0 \Rightarrow u = u_{cr}^D = \frac{\mu}{\rho a_1}, \tag{34}$$

$$\frac{\delta\eta_D}{\delta u} = 0 \Rightarrow u = u_p^D = 2 \frac{\mu}{\rho a_1} = 2u_{cr}^D. \tag{35}$$

Now it is possible to derive the peak efficiency of the system:

$$\eta_p^D = \eta^D(u_p^D) = \frac{-\lambda a_1^2}{6\gamma_2 a_3}. \tag{36}$$

To fully determine the features of the analyzed variant, it is necessary to define its high-efficiency bandwidth B^D . It is

$$\eta^D = 0.9\eta_p^D \Rightarrow \frac{u_2}{u_1} = \frac{\frac{2}{0.9}\rho a_1 \mu \pm \frac{\sqrt{0.4}}{0.9}\rho a_1 \mu}{(\rho a_1)^2}, \tag{37}$$

$$B^D = u_2 - u_1 = \sqrt{\frac{160}{81} \frac{\mu}{\rho a_1}} \approx 1.4u_{cr}^D \approx 0.7u_p^D. \tag{38}$$

Figure 4 depicts the relationship between efficiency η^D and flow speed u , represented by the function Equation (32), compared with an analogous relationship obtained through numerical integration of the model Equation (20) for the following initial conditions: $y_1(0) = 0.1, \dot{y}_1(0) = 0, n_1(0) = 0, y_2(0) = 0, \dot{y}_2(0) = 0, n_2(0) = 0$. Moreover, the figure shows the values characterizing the efficiency of the variant— $u_{cr}^D, u_p^D, \eta_p^D$, and B^D .

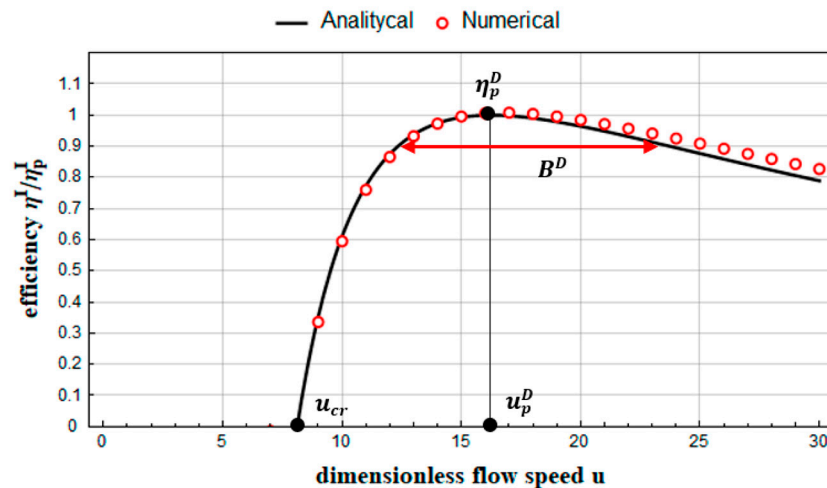


Figure 4. Efficiency characteristic of GEH2D for parameter values presented in Table 2.

Table 2. GEH2D system parameter values.

Parameter	Value
M	0.5
k_2	0.3
c_1	0.1
c_2	0.25
κ_1	0.9
κ_2	1.8
r_1	3
r_2	2
θ	1.3
a_1	2.3
a_3	−18
ρ	0.02

4. Comparison and Discussion

As suggested by Equations (34), (35), and (38), critical speeds, nominal speed, and high-efficiency bandwidths are interrelated in the same manner in both analyzed GEH

variants. Consequently, comparing the efficiency of these systems can only be achieved by comparing their peak efficiencies. Since the efficiency of both devices depends on their nominal speeds, it is necessary to compare systems with the same nominal speeds. The electrical damping of the linear system e^L will therefore be selected in such a way that this condition is satisfied. In the following derivation, it is assumed that the structural damping of the linear system c is equal to the structural damping c_1 of the damper connecting the lower mass of the GEH2D with the base, i.e., $c = c_1$. The shape of the flowing body, represented by the coefficients a_1 and a_3 , and the density of the fluid remain the same for all variants.

$$u_p^I = u_p^L, \tag{39a}$$

$$2 \frac{\mu + \gamma_2}{\rho a_1} = 2 \frac{e^L + c_1}{\rho a_1}, \tag{39b}$$

$$e^L = \gamma_2 + \mu - c_1. \tag{39c}$$

According to Equations (16) and (39c), the efficiency of a system with one degree of freedom with a nominal speed equal to the nominal speed of the GEH2D is equal to

$$\eta^L(u_p^D) = - \frac{(\mu - c_1)a_1^2}{6\mu a_3}. \tag{40}$$

The ratio of peak efficiencies of compared systems with the same nominal speed is therefore given by

$$\frac{\eta^L(u_p^D)}{\eta^D(u_p^D)} = \frac{s_1 + s_2}{s_1 + s_3}, \tag{41}$$

where

$$s_1 = \varepsilon_{T11} \left((k_2 + \theta^2 \delta_{D21}) (k_2 + \theta^2 \delta_{T21} - 2M\omega_1^2) + (c_2 + \theta^2 \varepsilon_{D21})^2 \omega_1^2 + M^2 \omega_1^4 \right), \tag{42a}$$

$$s_2 = M\omega_1^2 \left((k_2 \varepsilon_{D21} - c_2 \delta_{D21}) (\theta - 1) \theta + M\omega_1^2 (c_2 + \theta \varepsilon_{D21}) \right), \tag{42b}$$

$$s_3 = \theta^2 \varepsilon_{D21} \left(M\omega_1^2 (2k_2 (\theta - 1) + M\omega_1^2) + (c_2^2 \omega_1^2 + k_2^2) (\theta - 1)^2 \right). \tag{42c}$$

Clearly, according to Equation (41), the discussed system with two degrees of freedom will have greater efficiency than the reference system if and only if $s_3 > s_2$. For variant with only one lower transducer (Figure 3a), where $\varepsilon_{D21} = \delta_{D21} = 0$, this inequality takes the form

$$0 \not> c_2 M^2 \omega_1^4, \tag{43}$$

which implies that such a device cannot be more efficient than the reference system, regardless of its parameters. This conclusion contradicts the results presented in [25]. The reason for this discrepancy lies in the fact that in the cited work, the operating conditions of the compared systems were not standardized—the devices had different critical speeds and, consequently, different nominal speeds. Despite the unquestionable value of this article, the conclusion stated therein can be subject to questioning. In the case of the variant with only the upper transducer (Figure 3b), where $\varepsilon_{T11} = \delta_{T11} = 0$, the condition for efficiency improvement takes the following form:

$$\varepsilon_{D21} \not> \varepsilon_{D21} + c_2, \tag{44}$$

which indicates that this variant does not offer efficiency enhancement. Similarly, an identical and impossible-to-satisfy requirement is associated with the special case of the third variant, where there are two identical transducers, meaning $\varepsilon_{D11} = \varepsilon_{T21}$, $\delta_{D11} = \delta_{D21}$,

and $\theta = 1$. However, the inequality $s_3 > s_2$ can be satisfied for the most general variant—the one equipped with two different transducers. In this case, it can be reduced to the condition

$$(\theta - 1)\theta \left(\varepsilon_{D21}k_2^2(\theta - 1)\theta + c_2\delta_{D21}M\omega_1^2 + c_2^2\varepsilon_{D21}\omega_1^2(\theta - 1)\theta + \varepsilon_{D21}k_2M\omega_1^2(2\theta - 1) \right) > M^2\omega_1^4(c_2 - \varepsilon_{D21}(\theta - 1)\theta), \tag{45}$$

which, after substituting the solution of Equation (27), can be solved numerically for a chosen parameter. For the parameters presented in Table 2, solving the above inequality for θ results in obtaining a threshold value of approximately $\theta \approx 1.13$. An example of the efficiency characteristics of the GEH with e^L given by Equation (39c) and GEH2D is shown in Figure 5, where condition Equation (45) has been met by adopting parameters according to Table 2, with $\theta = 1.3 > 1.13$. It should be noted that parametric analysis does not allow one to indicate the optimal gain that the discussed system can provide. Determining this fact can be considered as a potential direction for further research.

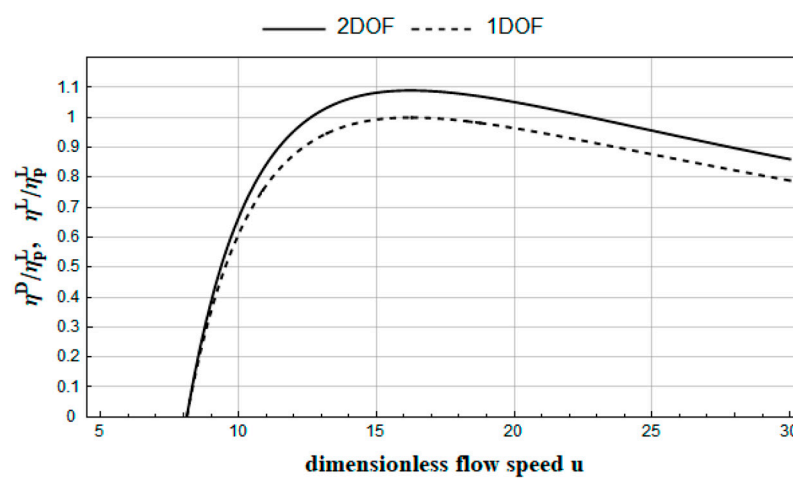


Figure 5. Comparison of GEH and GEH2D having equal nominal speeds.

5. Conclusions

The aim of the study was to investigate the efficiency of a galloping energy harvester with two degrees of freedom, considering its three variants, which differ in the number and location of electromechanical transducers. The realization of this objective commenced with the analysis of the reference variant with one degree of freedom. Utilizing the harmonic balance method, an approximate solution of the mathematical model of the system was derived, followed by the formulation of an expression describing the efficiency of the variant. Based on this, key criteria parameters were defined, providing comprehensive information about the variant’s efficiency: peak efficiency, high-efficiency bandwidth, critical speed, and nominal speed.

Subsequent sections of the study delineated the multitude of configurations that a system with two degrees of freedom can adopt. Three different subvariants of the device were characterized, differing from each other by the location and number of the electromechanical transducers. Parameters characterizing the efficiency of all subvariants were derived, demonstrating that the critical speed, nominal speed, and high-efficiency bandwidth are related to each other in the same manner as in the case of the reference system. It was then demonstrated that among the three indicated subvariants of the two-degree-of-freedom system, only the one with two transducers can be more efficient than the reference system.

Author Contributions: Conceptualization, F.S.; methodology, F.S.; software, F.S.; validation, R.S.; formal analysis, F.S. and R.S.; investigation, F.S.; resources, F.S.; data curation, F.S.; writing—original draft preparation, F.S.; writing—review and editing, R.S.; visualization, F.S.; supervision, R.S.; project

administration, F.S.; funding acquisition, R.S. All authors have read and agreed to the published version of the manuscript.

Funding: This research was funded by the Polish Ministry of Higher Education, grant number 0612/SBAD/3628.

Institutional Review Board Statement: Not applicable.

Informed Consent Statement: Not applicable.

Data Availability Statement: The data presented in this study are available in article.

Conflicts of Interest: The authors declare no conflict of interest.

References

1. Kumar, S.; Tiwari, P.; Zymbler, M. Internet of Things is a revolutionary approach for future technology enhancement: A review. *J. Big Data* **2019**, *6*, 111. [CrossRef]
2. Bladeless Vortex Official Site. Available online: <https://vortexbladeless.com> (accessed on 1 May 2024).
3. Den Hartog, J.P. *Mechanical Vibrations*, 4th ed.; McGraw-Hill: New York, NY, USA, 1956.
4. Barrero-Gil, A.; Alonso, G.; Sanz-Andrés, A. Energy harvesting from transverse galloping. *J. Sound Vib.* **2010**, *329*, 2873–2883. [CrossRef]
5. Ludlam, D.V. Optimal Energy Harvesting Form Vortex Induced Vibration and Transverse Galloping Vibrations. Ph.D. Thesis, Universidad Politécnica de Madrid, Madrid, Spain, 2017.
6. Ibarra, D.; Sorribes, F.; Alonso, G.; Meseguer, J. Transverse galloping of two-dimensional bodies having a rhombic cross-section. *J. Sound Vib.* **2014**, *333*, 2855–2865. [CrossRef]
7. Wang, J.; Tang, L.; Zhao, L.; Zhang, Z. Efficiency investigation on energy harvesting from airflows in HVAC system based on galloping of isosceles triangle sectioned bluff bodies. *Energy* **2019**, *172*, 1066–1078. [CrossRef]
8. Noel, J.; Yadav, R.; Li, G.; Daqaq, M. Improving the performance of galloping micro-power generators by passively manipulating the trailing edge. *Appl. Phys. Lett.* **2018**, *12*, 083503. [CrossRef]
9. Zhao, D.; Hu, X.; Tan, T.; Yan, Z.; Zhang, W. Piezoelectric galloping energy harvesting enhanced by topological equivalent aerodynamic design. *Energy Convers. Manag.* **2020**, *222*, 113260. [CrossRef]
10. Zhao, K.; Zhang, Q.; Wang, W. Optimization of Galloping Piezoelectric Energy Harvester with V-Shaped Groove in Low Wind Speed. *Energies* **2019**, *12*, 4619. [CrossRef]
11. Zheng, J.; Li, Z.; Zhang, H. Low-Wind-Speed Galloping Wind Energy Harvester Based on a W-Shaped Bluff Body. *Energies* **2024**, *17*, 958. [CrossRef]
12. Wang, J.; Ren, H.; Qin, W. High-performance piezoelectric wind energy harvester with Y-shaped attachments. *J. Appl. Phys.* **2019**, *181*, 645–652. [CrossRef]
13. Yuan, Y.; Wang, H.; Yang, C.; Sun, H.; Tang, Y.; Zhang, Z. Exploring the Potential of Flow-Induced Vibration Energy Harvesting Using a Corrugated Hyperstructure Bluff Body. *Micromachines* **2023**, *14*, 1125. [CrossRef]
14. Ewere, F.; Wang, G.; Frendi, A. Galloping Piezoelectric Energy Harvester with Bio-inspired Square Bluff Body. In Proceedings of the 23rd AIAA/AHS Adaptive Structures Conference Materials, Kissimmee, FL, USA, 5–9 January 2015.
15. Wang, J.; Sun, S.; Hu, G.; Yang, Y.; Tang, L.; Li, P.; Zhang, G. Exploring the potential benefits of using metasurface for galloping energy harvesting. *Energy Convers. Manag.* **2021**, *243*, 114414. [CrossRef]
16. Hai, W.; Sun, H.; Zhang, Z.; Tang, Y.; Yang, C.; Li, H. Improving the performance of galloping energy harvester with striped bluff body. *AIP Adv.* **2023**, *13*, 075019.
17. Abdelkefi, A.; Yan, Z.; Hajj, M.R. Nonlinear dynamics of galloping-based piezoaeroelastic energy harvesters. *Eur. Phys. J. Spec. Top.* **2013**, *222*, 1483–1501. [CrossRef]
18. Abdelkefi, A.; Yan, Z.; Hajj, M.R. Modeling and nonlinear analysis of piezoelectric energy harvesting from transverse galloping. *Smart Mater. Struct.* **2013**, *22*, 025016. [CrossRef]
19. Li, H.T.; Ren, H.; Cao, F.; Qin, W.Y. Improving the galloping energy harvesting performance with magnetic coupling. *Int. J. Mech. Sci.* **2023**, *237*, 107785. [CrossRef]
20. Zhang, H.; Zhang, L.; Wang, Y.; Yang, X.; Song, R.; Sui, W. Modeling and experimental investigation of asymmetric distance with magnetic coupling based on galloping piezoelectric energy harvester. *Smart Mater. Struct.* **2022**, *31*, 065007. [CrossRef]
21. Sarbinowski, F.; Starosta, R. Assessment of the role of structural nonlinearity in galloping energy harvesters. *Vib. Phys. Syst.* **2021**, *32*, 2021209.
22. Alhadidi, A.; Abderrahmane, H.; Daqaq, M. Exploiting stiffness nonlinearities to improve flow energy capture from the wake of a bluff body. *Phys. D Nonlinear Phenom.* **2016**, *337*, 30–42. [CrossRef]
23. Yang, K.; Yang, K.; Wang, J.; Wang, J.; Yurchenko, D. A double-beam piezo-magneto-elastic wind energy harvester for improving the galloping-based energy harvesting. *Appl. Phys. Lett.* **2019**, *115*, 193901. [CrossRef]
24. Wang, J.; Geng, L.; Zhou, S.; Zhang, Z.; Lai, Z. Design, modeling and experiments of broadband tristable galloping piezoelectric energy harvester. *Acta Mech. Sin.* **2020**, *36*, 592–605. [CrossRef]

25. Lan, C.; Tang, L.; Hu, G.; Qin, W. Dynamics and performance of a two degree-of-freedom galloping-based piezoelectric energy harvester. *Smart Mater. Struct.* **2019**, *28*, 045018. [[CrossRef](#)]
26. Hu, G.; Wang, J.; Qiao, H.; Zhao, L.; Li, Z.; Tang, L. An Experimental Study of a Two-Degree-of-Freedom Galloping Energy Harvester. *Int. J. Energy Res.* **2020**, *45*, 3365–3374. [[CrossRef](#)]
27. Hu, G.; Wang, J.; Tang, L. A Comb-Like Beam based Piezoelectric System for Galloping Energy Harvesting. *Mech. Syst. Signal Process.* **2021**, *150*, 107301. [[CrossRef](#)]
28. Hu, G.; Liang, J.; Tang, L.; Wang, J. Improved Theoretical Analysis and Design Guidelines of a Two-Degree-of-Freedom Galloping Piezoelectric Energy Harvester. *J. Intell. Mater. Syst. Struct.* **2021**, *33*, 210–230. [[CrossRef](#)]
29. Zhao, L.; Tang, L.; Yang, Y. Enhanced piezoelectric galloping energy harvesting using 2 degree-of-freedom cut-out cantilever with magnetic interaction. *Jpn. J. Appl. Phys.* **2014**, *53*, 060302. [[CrossRef](#)]

Disclaimer/Publisher’s Note: The statements, opinions and data contained in all publications are solely those of the individual author(s) and contributor(s) and not of MDPI and/or the editor(s). MDPI and/or the editor(s) disclaim responsibility for any injury to people or property resulting from any ideas, methods, instructions or products referred to in the content.